AD-A192 342 OPTICAL CORRELATION USING THE MAGNETO-OPTIC DEVICE(U) 1/1
LITTON SYSTEMS INC VAN NUYS CALIF DATA SYSTEMS DIV
W E ROSS DEC 87 AFATL-TR-87-26 F08635-85-C-0137
UNCLASSIFIED F/G 17/5 NL

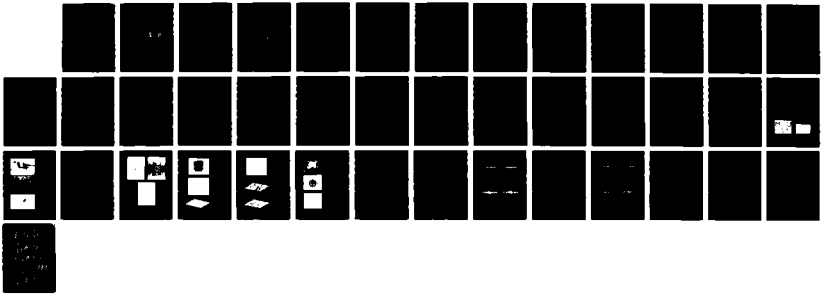

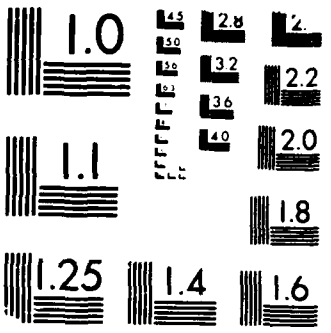

AFATL-TR-87-26

Optical Correlation Using the Magneto-Optic Device

William E Ross

LITTON DATA SYSTEMS
8000 WOODLEY AVENUE
VAN NUYS, CALIFORNIA 91409

DECEMBER 1987

FINAL REPORT FOR PERIOD OCTOBER 1985-FEBRUARY 1987

AIR FORCE ARMAMENT LABORATORY
Air Force Systems Command ▮ United States Air Force ▮ Eglin Air Force Base, Florida

UNCLASSIFIED
SECURITY CLASSIFICATION OF THIS PAGE

AD-A192342

REPORT DOCUMENTATION PAGE

Form Approved
OMB No. 0704-0188

1a. REPORT SECURITY CLASSIFICATION Unclassified	1b. RESTRICTIVE MARKINGS
2a. SECURITY CLASSIFICATION AUTHORITY	3. DISTRIBUTION/AVAILABILITY OF REPORT Approved for public release; distribution is unlimited.
2b. DECLASSIFICATION/DOWNGRADING SCHEDULE	
4. PERFORMING ORGANIZATION REPORT NUMBER(S)	5. MONITORING ORGANIZATION REPORT NUMBER(S) AFATL-TR-87-26
6a. NAME OF PERFORMING ORGANIZATION Litton Industries 6b. OFFICE SYMBOL (If applicable)	7a. NAME OF MONITORING ORGANIZATION Air-to-Surface Guidance Branch Advanced Guidance Division
6c. ADDRESS (City, State, and ZIP Code) Litton Data Systems 8000 Woodley Avenue Van Nuys, CA 91409	7b. ADDRESS (City, State, and ZIP Code) Air Force Armament Laboratory Eglin AFB, FL 32542-5434
8a. NAME OF FUNDING/SPONSORING ORGANIZATION Advanced Guidance Division 8b. OFFICE SYMBOL (If applicable) AFATL/AGS	9. PROCUREMENT INSTRUMENT IDENTIFICATION NUMBER F08635-85-C-0137
8c. ADDRESS (City, State, and ZIP Code) Air Force Armament Laboratory Eglin AFB, FL 32542-5434	10. SOURCE OF FUNDING NUMBERS PROGRAM ELEMENT NO.: 61101F; PROJECT NO.: ILIR; TASK NO: 85; WORK UNIT ACCESSION NO.: 19

11. TITLE (Include Security Classification)
Optical Correlation Using the Magneto-Optic Device

12. PERSONAL AUTHOR(S)
William E. Ross

13a. TYPE OF REPORT	13b. TIME COVERED	14. DATE OF REPORT (Year, Month, Day)	15. PAGE COUNT
Final	FROM Oct 85 TO Feb 87	December 1987	43

16. SUPPLEMENTARY NOTATION
Availability of this report is specified on verso of front cover.

17. COSATI CODES			18. SUBJECT TERMS (Continue on reverse if necessary and identify by block number)
FIELD	GROUP	SUB-GROUP	Optical Detection Magneto Optic Effect
17	05		
20	06		

19. ABSTRACT (Continue on reverse if necessary and identify by block number)

This report describes binary filters and applications of the Magneto-Optic Device (MOD) to pattern recognition. Three issues concerning use of the MOD in pattern recognition are reported herein. They are:

a. The use of the MOD as an input device and as a spatial filter in a Vander Lugt correlator.

b. Algorithms to generate binary filters for multiple images recognition.

c. The use of MOD for multiple bit-slice correlations.

20. DISTRIBUTION/AVAILABILITY OF ABSTRACT	21. ABSTRACT SECURITY CLASSIFICATION	
☐ UNCLASSIFIED/UNLIMITED ☒ SAME AS RPT. ☐ DTIC USERS	Unclassified	
22a. NAME OF RESPONSIBLE INDIVIDUAL James M. Kirkpatrick	22b. TELEPHONE (Include Area Code) (904) 882-5252	22c. OFFICE SYMBOL AFATL/AGS

DD Form 1473, JUN 86 *Previous editions are obsolete.*

PREFACE

The work reported herein was conducted by Litton Data Systems, 8000 Woodley Avenue, Van Nuys, California 91409, under contract F08635-85-C-0137 with the Air Force Armament Laboratory, Eglin Air Force Base, Florida 32542-5434. Dennis Goldstein (AFATL/AGS) and James Kirkpatrick (AFATL/AGS) managed the program for the Armament Laboratory. The work of Litton Data Systems was under the direction of Mr. William Ross. The program was conducted during the period from October 1985 to February 1987. This effort was accomplished under Project ILIR 85-19.

The work described herein was performed by Demetri Psaltis and Fai Mok of the California Institute of Technology, Department of Electrical Engineering, Pasadena, California. Dr. Psaltis of Caltech was the principal investigator.

TABLE OF CONTENTS

LIST OF FIGURES

LIST OF FIGURES (CONCLUDED)

SECTION I
INTRODUCTION

Ever since Vander Lugt demonstrated optical matched filtering in 1964 (Reference 1), the main stream of optical pattern recognition has been correlation type image recognition. This field of research, however, has had limited success in practical systems. One of the most important reasons was the lack of a suitable spatial light modulator (SLM). The development of the Magneto-Optic Device (MOD) has opened up new possibilities. This report addresses the issues of the feasibility of using the Magneto-Optic Device as a spatial light modulator for correlation, and the performance of binary filters versus linear filters in terms of output signal to noise ratio (SNR) and storage capacity..

SECTION II
BINARY CORRELATORS

A schematic diagram of the classic Vander Lugt correlator is shown in Figure 1. The real-time implementation of this processor requires two MODs. The first is used to record the input image placed at plane P_1, whereas the second MOD, placed at plane P_2, records the Fourier transform hologram of the reference image. The correlation output is obtained at plane P_3.

Since the MOD is a binary device, the effects of thresholding the input image and the Fourier transform (FT) of the reference image have to be evaluated. The performance measure that is adopted here is SNR, the signal (correlation peak) to noise (additive noise and average side-lobe) ratio.

The first investigation involves the effect of thresholding the input image on the SNR. Let f(i,j) be the image to be recognized. Assume f(i,j) to be a discrete sequence of independent, identically distributed Gaussian random variables with zero mean and variance σ_f^2. The input image to the correlator is the sum of f(i,j), the image to be recognized, and n(i,j), the additive noise. Here it is also assumed n(i,j) to be an independent, discrete sequence of Gaussian random variables with zero mean and variance σ_n^2. The thresholded image is defined as

$$\hat{f}(i,j) = \begin{cases} 1, & \text{if } f(i,j) + n(i,j) \geq 0; \\ -1, & \text{if otherwise.} \end{cases} \qquad (1)$$

Assumed for now is a joint transform architecture where both the input and reference images are recorded on MODs. In this

case, the reference image h(i,j) is obtained by thresholding f(i,j):

$$h(i,j) = \begin{cases} 1, & \text{if } f(i,j) \geq 0; \\ -1, & \text{if otherwise.} \end{cases} \qquad (2)$$

The correlation between the thresholded input and reference images is then given by

$$g(i',j') = \sum_{i}^{N} \sum_{j}^{N} f(i,j)h(i+i',\ j+j') \qquad (3)$$

The signal to noise ratio, defined as

$$SNR' = \frac{E^2\,[g(0,0)]}{\text{var}\,[g(i',j'],} \qquad i',j' = 0 \qquad (4)$$

can be shown to be

$$SNR' = N^2\left[\frac{1}{2} + \frac{1}{\pi}\tan^{-1}(SNR_{in})\right]^2 \qquad (5)$$

where $SNR_{in} = \dfrac{\sigma_f}{n^{\sigma}}$

In order to see the effect of thresholding the input image, compare SNR' with the signal to noise ratio that is obtained if the input and reference images are not thresholded. It can be shown that in this case

$$SNR = \frac{N^2 \, SNR_{in}^2}{1 + SNR^2}. \qquad (6)$$

The two SNRs are plotted in Figure 2 as a function of SNR_{in}^2. As can be readily observed from the plot, the correlator with input image thresholded is only marginally degraded for high input SNR.

The effect of thresholding the Fourier transform of the reference image in a Vander Lugt correlation in which the FT hologram is recorded on an MOD is explored. (Since the Fourier transform of an image is generally complex, what is meant by thresholding the FT is that the real part of the FT of an image pattern is hard-limited.) Suppose $F_R(u,v) + jF_I(u,v)$ is the FT of the image pattern to be recognized. The computer generated hologram (CGH), which is used as the filter for recognition, is then formed using the following algorithm:

$$H(u,v) = \begin{cases} +1, & \text{if } F_R(u,v) \geq 0; \\ -1, & \text{if otherwise.} \end{cases} \qquad (7)$$

The correlation output g(x,y) is then given by

$$g(x,y) = \int_{-v_1}^{v_1} \int_{-u_1}^{u_1} || F_R(u,v) || \exp[j2\pi(ux + vy)] \, dudv$$

$$+ \int_{-v_1}^{v_1} \int_{-u_1}^{u_1} F_i(u,v) \, H(u,v) \exp[j2\pi(ux + vy)] \, dudv \qquad (8)$$

The first term on the right-hand side of Equation 8 is the Fourier transform of a real, positive quantity and will,

therefore, give a strong correlation peak at (x,y) = (0,0). The expected value of the second term is zero. Hence, a binary CGH of this type can be used for recognition. Note that the usage of such an on-axis CGH is possible only because the bipolar nature of the CGH eliminates the necessity of bias removal.

The loss in SNR that results from the use of this suboptimum filter is estimated. Let the image f(x,y) to be recognized be a Gaussian white process with zero mean and variance σ_f^2. Suppose f(x,y) is contaminated by an additive Gaussian white noise n(x,y), independent of f(x,y), with zero mean and variance σ_n^2. For $\sigma_n >> \sigma_f$, it can be shown (Reference 2) that:

$$SNR = \frac{SBP}{\pi} \left(\frac{\sigma_f}{\sigma_n} \right)^2 \qquad (9)$$

where SBP is the space-bandwidth product. Recall that the SNR of the conventional matched filter is the product of the SBP and the input SNR. Thus, the SNR is only reduced by a factor of π when a quantized hologram replaces a matched filter. It is difficult to find a closed form expression for the SNR for sufficiently low noise ($\sigma_f >> \sigma_n$). However, numerical evaluations for low SBP indicate that the performance of the quantized FT filter, while always slightly inferior to that of the matched filter, approaches the performance of the matched filter as the input SNR becomes large (Figure 3). Experimental evidence also supports this result for higher SBP. The results of two optical correlation experiments using the MOD programmed with quantized FT holograms are shown in Figures 4 and 5.

The MOD can also be used in the Fourier plane of a two-dimensional holographic acousto-optic image correlator. Figure 6 shows the schematic diagram of the corresponding architecture. The cross-correlation is obtained by taking the inverse Fourier transform of the product of the Fourier transforms of the input image and the reference in the abscissa while performing a shift and integrate type correlation in the ordinate. The procedure for producing the correlation can be described mathematically by the following equation:

$$G(u,y) = \sum_{n}^{N} F(u,\ nd + y)\ H(u,nd) \tag{10a}$$

and

$$g(x,y) = \int G(u,y)e^{j2\pi ux}\ dx, \tag{10b}$$

where $F(u,nd + d)$ and $H(u,nd)$ are the one-dimensional Fourier transforms of the input image and the reference, respectively. As it is apparent from the equation, the algorithm for generating the hologram is different from the one described by Equation 7. Since the correlation operation of this architecture involves space integration (implemented by the one-dimensional Fourier transform) in one dimension and time integration (implemented by the time delay integrating mode of the charge coupled device (CCD)) in the other, the hologram is generated by quantizing the real part of only the one-dimensional Fourier transform of the reference image; that is:

$$H(u,nd) = \begin{cases} +1, & \text{if } F(u,nd) \geq 0; \\ -1, & \text{if } F(u,nd) < 0 \end{cases} \tag{11}$$

A preliminary experiment of correlating the letter X and the filter generated using the above scheme was performed. The result is shown in Figure 7.

SECTION III
BINARY ROTATION INVARIANT FILTERS

Mathematically, any pattern $f(r,\theta)$ can be decomposed into an infinite sum of its circular harmonics,

$$f(r,\theta) = \sum_{n=-\infty}^{\infty} f_n(r)e^{-jn\theta}, \tag{12a}$$

where

$$f_n(r) = \int f(r,\theta)e^{jn\theta}d\theta. \tag{12b}$$

Thus, if the pattern is correlated with any component of its circular harmonics $f_n(r)e^{-jn\theta}$, the magnitude of the output is rotation invariant (Reference 3). Furthermore, if any component of the circular harmonics is recorded on a Fourier transform hologram, the resulting filter is also shift invariant.

Bipolar filters can be formed by using an algorithm similar to that described by Equation 7, namely:

$$H(s,w) = \begin{cases} +1, & \text{if } \mathrm{Re}[F_n(s,w)] \geq 0; \\ -1, & \text{otherwise,} \end{cases} \tag{13}$$

where $F_n(s,w)$ is the Fourier transform of the nth order circular harmonics of the input image. Computer generated bipolar filters were obtained from the first two orders of circular harmonics of the letter A. Numerical correlations of the letters A, B, C, and D and the bipolar CGHs were evaluated. The result are presented in Figure 8. The intra-class recognition using the zeroth order circular

harmonics is remarkable. However, the inter-class discrimination performance is not satisfactory. In order to obtain good discrimination performance, cross-correlations using binary filters generated from different circular harmonics have to be evaluated. A compromise between the inter- and intra-class discrimination performance will determine which binary filter is to be used. The result of the optical implementation of the cross-correlation of the letter A and the binary Fourier transform filter, recorded on a 128 by 128 MOD, of the A's zeroth order circular harmonics is presented in Figure 9. Figure 9(a) is the image of the rotation-invariant binary filter, whereas Figure 9(b) is the reconstruction of the binary filter. Note that both of them are circularly symmetric. Figure 9(c) is the correlation output. Note that the peak is very sharp and is located at the center of the dc pass of the A, just as the simulation predicted. Rotation of the input object did not cause the peak to diminish in amplitude as expected.

SECTION IV
GENERALIZED BINARY FILTERS

This section examines the possibility of designing linear bipolar filters for recognizing multiple objects. One immediate extension of such a design, if it can be done, is to incorporate information corresponding to multiple versions of a certain object in a filter to achieve invariance (e.g., rotation and/or scale). Two schemes that may accomplish this goal are investigated as described below.

The first scheme is a derivative of the well known 2-category perceptron invented in the 1960's (Reference 4). Basically, a 2-category linear perceptron is a machine consisting of a weight pattern $\underline{w}$ trained by a certain algorithm utilizing the set of all input patterns $\{\underline{f}_m\}$ such that the output

$$g = \text{sgn}\left[\sum_{i,j}^{N^2} w(i,j) f_m(i,j)\right] = \begin{cases} +1 & \text{if } f_m \text{ belongs to } \Psi; \\ -1 & \text{otherwise.} \end{cases} \quad (14)$$

Attention is here confined to one of the simplest perceptron training algorithms, which is as follows: the set of input patterns is arranged as a repetitive sequence of patterns, i.e., $\{\underline{f}^1, \underline{f}^2, \ldots, \underline{f}^M, \underline{f}^1 \ldots\}$. The weight vector is trained by the elements from the sequence one at each time,

$$\underline{w}^{k+1} = \underline{w}^k + \alpha^k \underline{f}^k; \; \underline{w}^1 = \text{some initial vector,} \quad (15a)$$

where

$$\alpha^k = \begin{cases} +1 & \text{if } g^k = \text{sgn}\,[\underline{w}^k \cdot \underline{f}^k] = -1 \text{ and } \underline{f}^k \in \Psi; \\ -1 & \text{if } g^k = +1 \text{ and } \underline{f}^k \notin \Psi; \\ 0 & \text{otherwise.} \end{cases} \tag{15b}$$

A solution vector is found when the right response is obtained for each input vector.

A bipolar perceptron can be defined by modifying the linear perceptron simply by replacing $\underline{w}$ by a bipolar weight pattern. The training algorithm can also be modified to

$$\underline{w}^{k+1} = \text{sgn}\,[\underline{w}^k + \alpha^k \underline{f}^k] \tag{16}$$

The result of the rate of convergence of a binary perceptron trained by using the above scheme is shown in Figure 10. An ordinate reading of 10^4 iterations means the binary perceptron did not converge within 10^4 steps. Even though a convergence proof does not exist, preliminary computer simulations indicate that a binary solution weight pattern can be obtained provided the dimensionality N is high enough. The statistical capacity with N = 16 is shown in Figure 11. Note that the capacity curve starts to roll off at approximately M, the number of stored vectors equal to 2N/3, whereas the capacity curve of a linear perceptron (not shown) does not roll off until M = N. This can be explained by the fact that the solution region of a linear perceptron may not contain a binary point. In such a case, a binary vector does not exist which classifies all input vectors correctly.

The second scheme that can be used to recognize multiple patterns is described below. For ease of comparison, the ordinary (non-bipolar) linear filter of the second scheme, designed for the desired purpose, is first analyzed. Consider the following algorithm: the operation to be performed is given as

$$g = \operatorname{sgn}\left[\sum_{i,j}^{N^2} h(i,j) f_m(i,j)\right] = \begin{cases} +1 & \text{if } f_m \text{ belongs to } \Psi; \\ -1 & \text{otherwise.} \end{cases} \tag{17}$$

where Ψ is the class of objects to be recognized. The filter $h(i,j)$ is generated by forming a weighted sum of all the input patterns, i.e.,

$$h(i,j) = \sum_{m'}^{M} a_{m'} f_{m'}(i,j) \tag{18a}$$

where

$$a_{m'} = \begin{cases} +1, & \text{if } f_{m'} \text{ belongs to } \Psi; \\ -1, & \text{otherwise,} \end{cases} \tag{18b}$$

To see that the above scheme is capable of recognizing multiple objects, rewrite Equation 17 as

$$g = \operatorname{sgn}\left[\alpha_m N^2 f_m^2(i,j) + \sum_{i,j}^{N^2} \sum_{m' \neq m}^{M} a_{m'} f_m(i,j)\, f_{m'}(i,j)\right] \tag{19}$$

The right-hand side of Equation 19 is composed of two terms, namely, the signal (first) term and the noise (second) term.

Provided that the signal term is sufficiently large compared to the noise term, the correct response is expected.

The next task is to obtain a theoretical estimate of the capacity of the filter. The capacity is defined to be the number of vectors M_c that can be stored in a filter with vanishingly small probability of error for sufficiently large dimensionality N. Assuming $f_m(i,j)$ to be a discrete sequence of bipolar-valued independent random variables, i.e.,

$$\begin{cases} P[f_m(i,j) = 1] = P[f_m(i,j) = 1] = 1/2; \\ P[f_m(i,j) \mid f_{m'}(i',j')] = P[f_m(i,j)], \end{cases} \tag{20}$$

it can be shown that

$$M_c \simeq \frac{N^2}{8 \ln N}. \tag{21}$$

Shift invariance can be incorporated into this system by modifying the operation to be

$$g(i',j') = \operatorname{sgn}\left[\sum_{i,j}^{N^2} h(i,j) f_m(i+i',\ j+j')\right] \tag{22}$$

$$= \begin{cases} +1 & \text{if } f_m \text{ belongs to } \Psi; \\ -1 & \text{otherwise.} \end{cases}$$

In such case, the capacity M_c can be shown to be

$$M_c \simeq \frac{N^2}{16 \ln N}. \tag{23}$$

The digitally computed correlations of random sequences (statistics given by Equation 20) and the linear weighted-sum filter with different number of vectors stored are shown in Figure 12. It can be seen from the simulated results that as the number of vectors stored in a filter increases, so do the magnitudes of the sidelobes. This phenomenon accounts for the limit of the number of vectors that can be stored in a weighted-sum filter. The histogram of capacity with dimensionality N equal 128 is shown in Figure 13. The mean of the histogram agrees with the theoretical result.

For the bipolar analog of the above scheme, consider the same operation given by Equation 17. In this case, the filter is generated by bipolarizing the filter given by Equation 18. It is given as follows,

$$h(i,j) = \text{sgn}\left[\sum_{m'}^{M} \alpha_{m'} f_{m'}(i,j)\right] . \tag{24}$$

Using the same statistics for the stored vectors, it can be shown that the capacity of a bipolar weighted sum filter is only reduced by a factor of $\pi/2$. Thus

$$M_b \simeq \frac{2}{\pi} \frac{N^2}{16 \ln N} , \tag{25}$$

for filters with shift invariance incorporated, and

$$M_b \simeq \frac{2}{\pi} \frac{N^2}{8 \ln N} , \tag{26}$$

for filters without. Computer simulated correlations of random vectors and the bipolar filter formed by the above algorithm

are shown in Figure 14. Note that the magnitude of the peak decays as the number of vectors stored increases in this case. This phenomenon is understandable, since as M increases, the relative information of each vector stored in the filter decreases. The histogram of capacity of the corresponding bipolar filter is shown in Figure 15. The mean of the histogram agrees with the theoretical result.

SECTION V
MULTIPLE BITS CORRELATORS

Conventional matched filtering can be implemented by utilizing a binary device such as the MOD. Let the input image be f(i,j). The reference image h(i,j) can be approximated by a weighted sum of binary numbers as the following

$$h(i,j) = \sum_{k=0}^{M} h_k (i,j) 2^k . \qquad (27)$$

The correlation output is thus given by

$$g(i',j') = \sum_{k=0}^{K} 2^k \left[\sum_{i,j}^{n^2} f(i+i',\ j+j')\ h_k(i,j) \right], \qquad (28)$$

The term included in the brackets is simply the correlation of the input image and a binary filter. Thus, the final output will be the sum of all the K weighted correlations, each being computed separately.

One way to implement this scheme is to have a setup of multiple MODs, each performing a bit-slice correlation with the input image. All the correlations are weighted properly and are then summed up interferometrically. This implementation has the drawback of having to use multiple MODs. If the Vander Lugt correlation is to be computed, a total of 2K MODs is required (K MODs for the real part of the FT of h(i,j) and another K MOD for the imaginary part).

Another way to implement the bit-slice scheme is to compute the bit-slice correlation in time by updating the MODs (two are required in this case) with different bit planes of the reference image. The final output is obtained by accumulating all the properly weighted correlations at the output detector. The tradeoff here is that it requires K times as long to perform a conventional correlation as it takes to compute a bit-slice correlation. The result of the computer simulation of the second method of implementation is shown in Figure 16. Note that the SNR of the final output differs from the first bit-slice correlation by a factor of approximately three. In view of this and similar results, and in addition, the knowledge gained from the analysis of the previous sections, it is believed that the gain in the output performance by computing bit-slice correlation does not rightfully compensate the increase in cost, difficulty and complexity.

SECTION VI
CONCLUSION

This report has shown that the performance, in terms of output SNR and storage capacity, of binary correlation filters does not severely degrade when compared to conventional correlation filters. As a matter of fact, bipolar spatial light modulators (SLMs) are free of the problems of limited dynamic range and non-linearity. However, binary filters are not without other problems besides those mentioned earlier. Many issues still remain to be researched, for instance, how a binary filter is optimized. How a binary perceptron is trained to recognize multiple objects is another example. For a certain set of data, a binary filter which will make the right decision in recognition may not exist at all. It is, nevertheless, the authors' expectation that the probability of having such a binary filter approaches one for sufficiently high dimensionality.

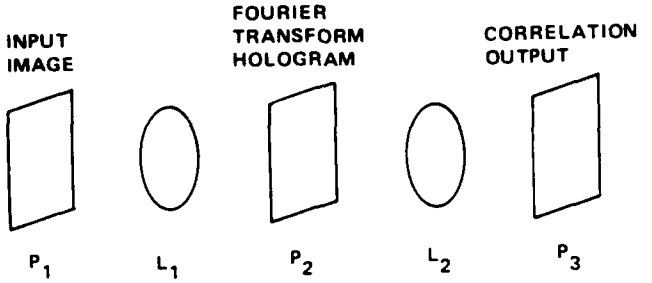

Figure 1. Vander Lugt Correlator

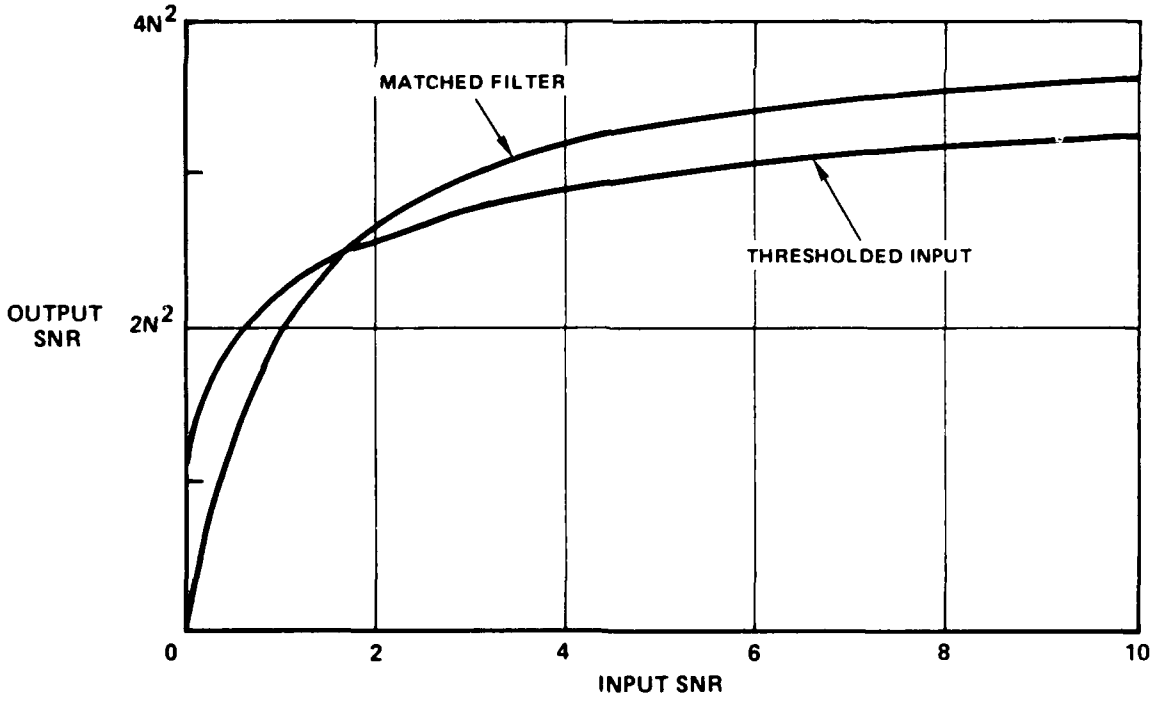

Figure 2. Output vs Input SNRs for the Binary and Conventional Correlators

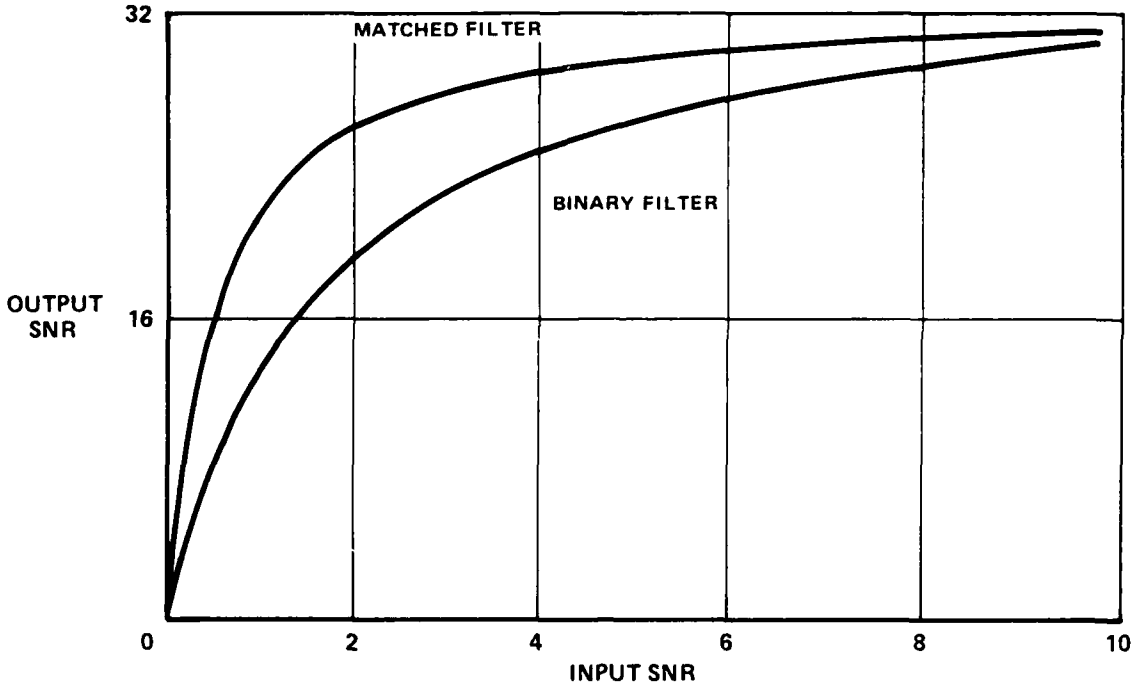

Figure 3. Output vs Input for a Correlator with a Binary Spatial Filter (The SNR of the Conventional Correlator is also Plotted for Comparison)

(a) (b)

Figure 4. Optical Correlation Using the Binary CGH of the Letter O

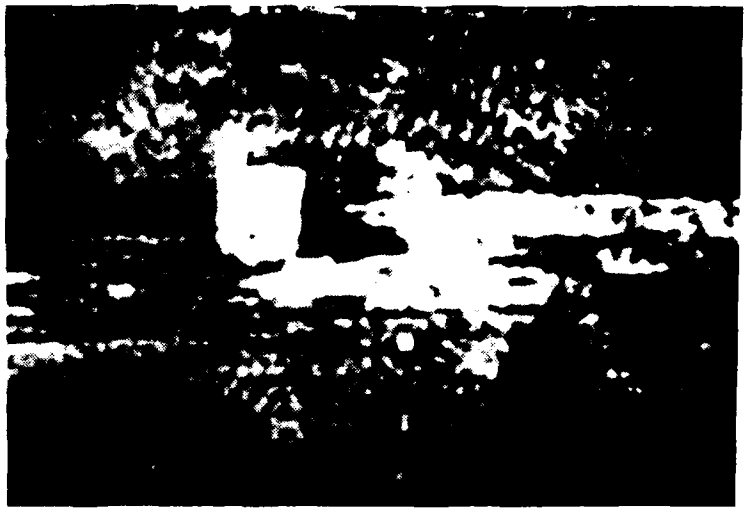

(a) IMAGE OF POWER PLANT

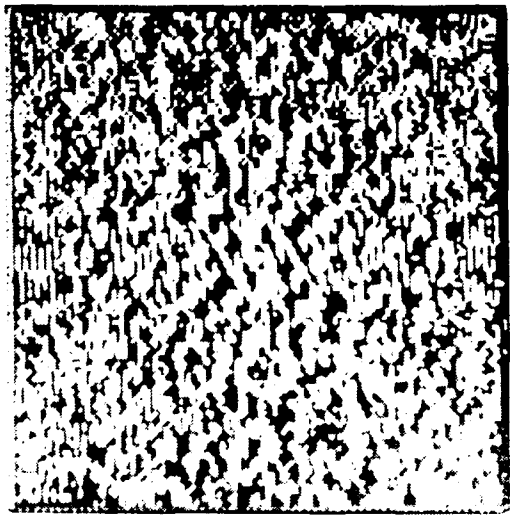

(b) BINARY OF CGH OF (a)

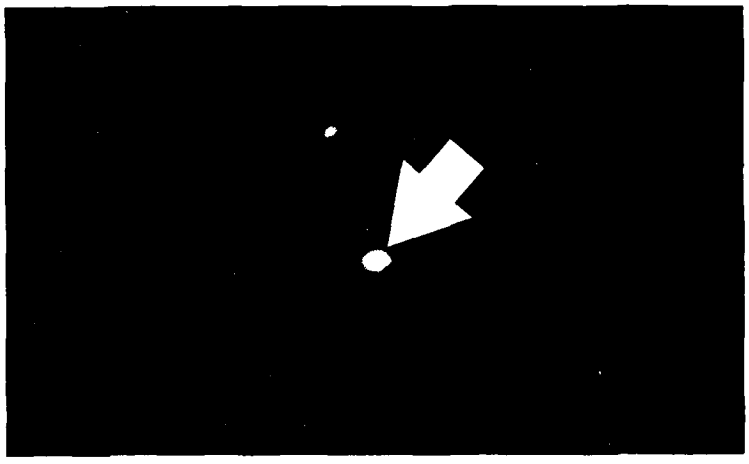

(c) OPTICAL CORRELATION RESULT OF (a) AND (b)

Figure 5. Optical Correlation Using the Binary CGH of an Image of a Power Plant

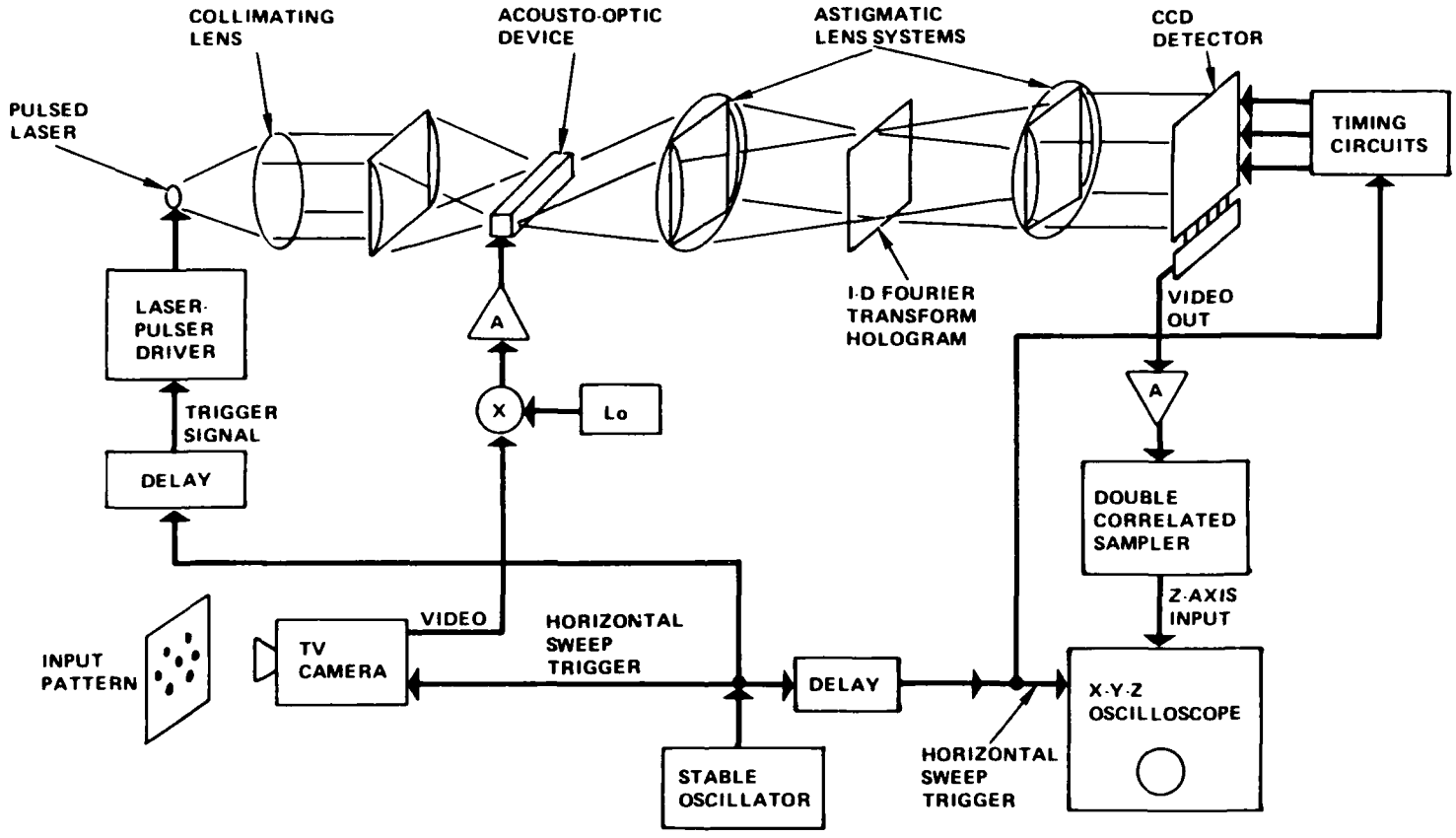

Figure 6. Holographic Acousto-Optic Image Correlator

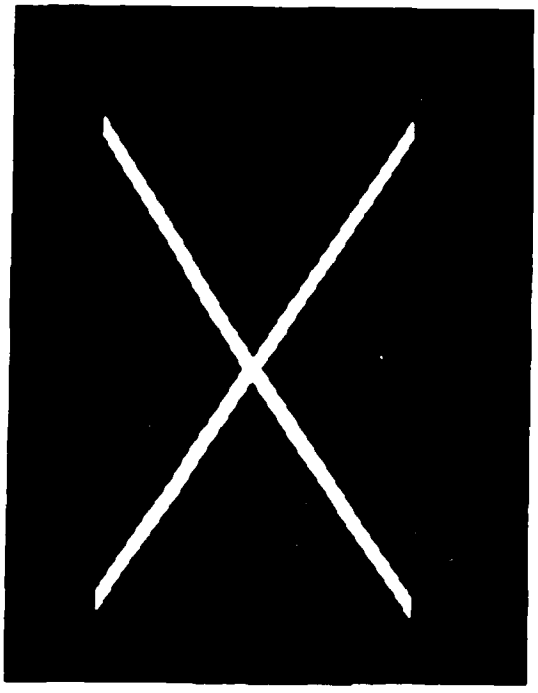

(a) INPUT

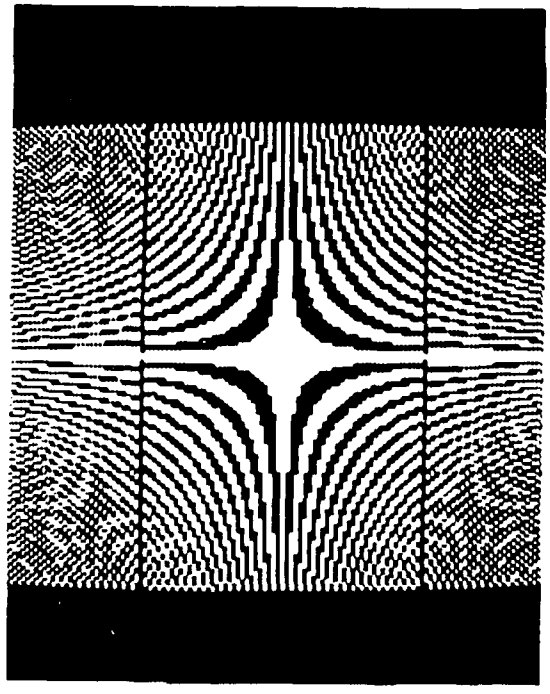

(b) HOLOGRAM

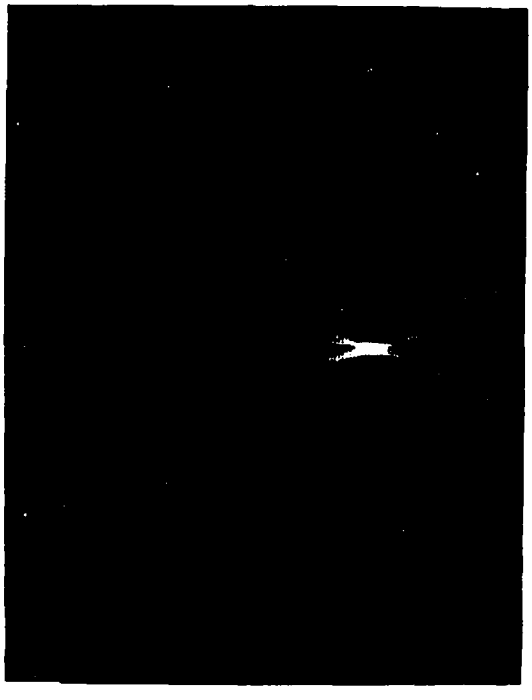

(c) CORRELATION OUTPUT

Figure 7. Experimental Demonstration of the Holographic Acoustic Correlator with a Programmable Magneto-Optic Device

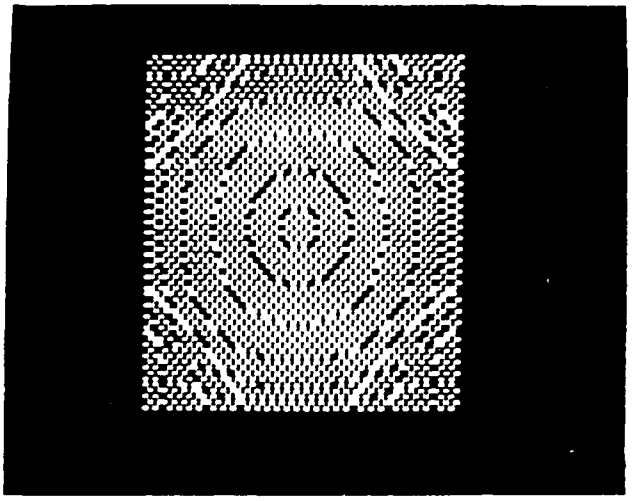

(a) ZEROTH ORDER CIRCULAR HARMONIC BINARY CGH

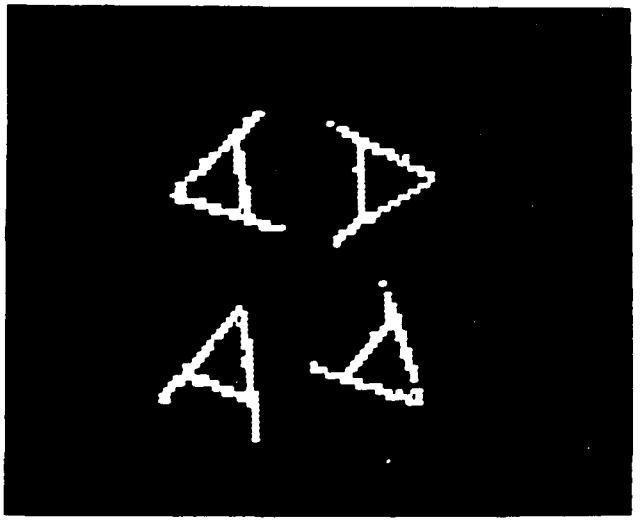

(b) IMAGE OF 4 As OF DIFFERENT ORIENTATION

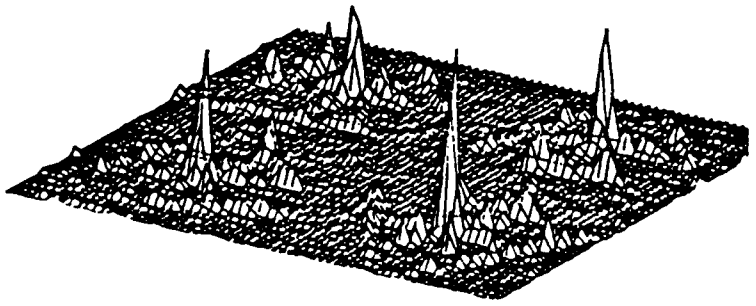

(c) COMPUTER SIMULATED CORRELATION RESULT OF (a) AND (b)

Figure 8. Optical Correlation Using Binary CGH of the Letter A

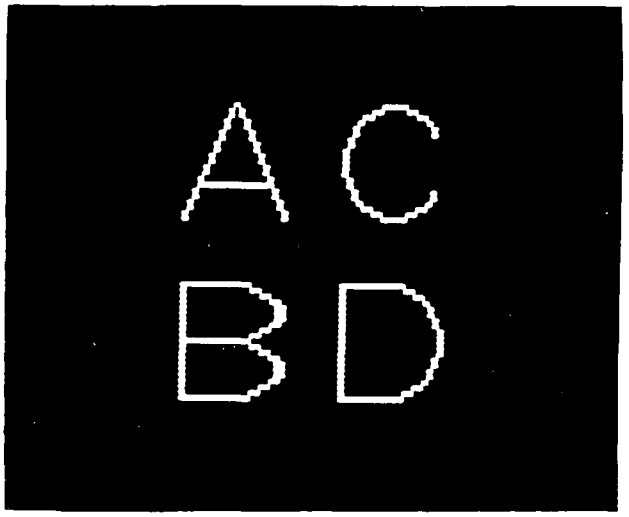

(d) IMAGE OF THE LETTERS A, B, C AND D

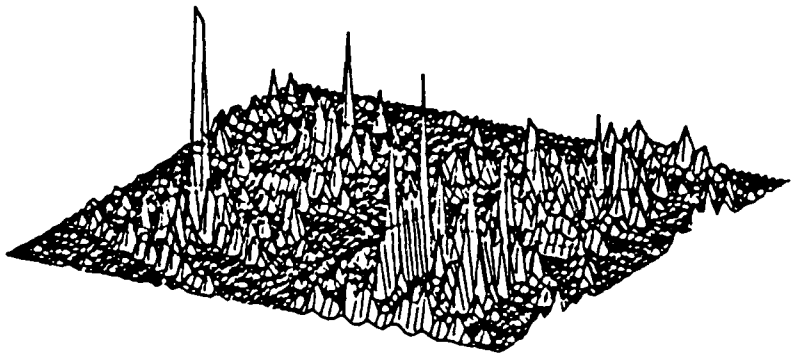

(e) COMPUTER SIMULATED CORRELATION RESULT OF (a) AND (d)

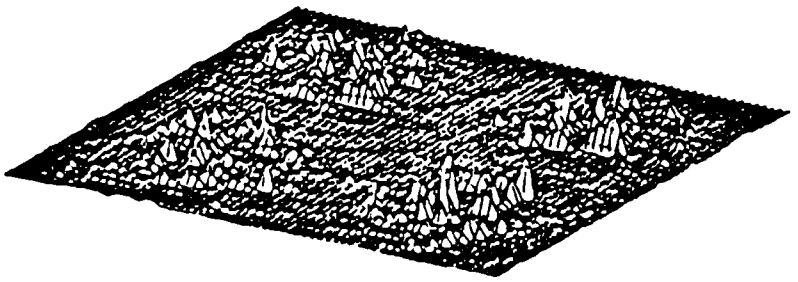

(f) COMPUTER SIMULATED CORRELATION RESULT OF (d) AND THE FIRST ORDER CIRCULAR HARMONIC BINARY CGH

Figure 8. Optical Correlation Using Binary CGH of the Letter A (Concluded)

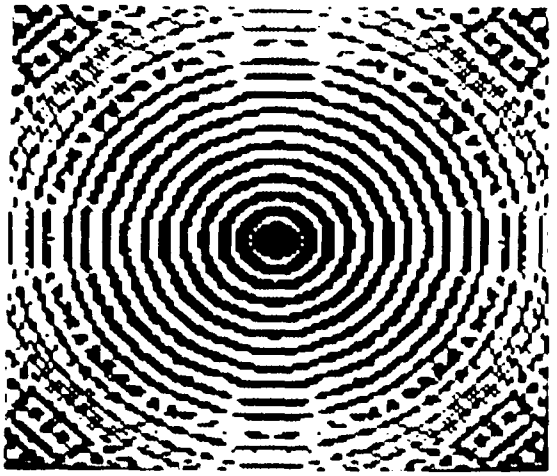

(a) BINARY FOURIER TRANSFORM HOLOGRAM OF THE ZEROTH ORDER CIRCULAR HARMONICS OF THE LETTER A

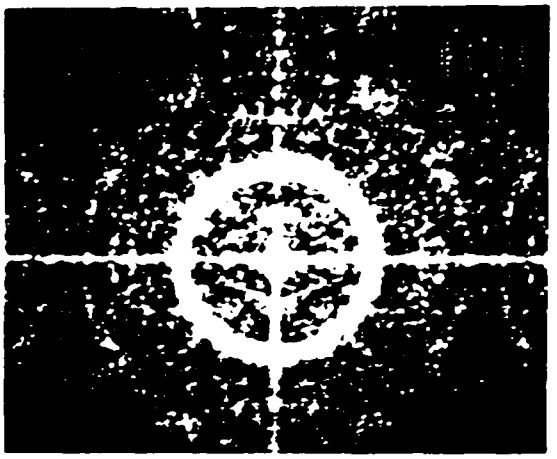

(b) RECONSTRUCTION OF THE BINARY HOLOGRAM (a)

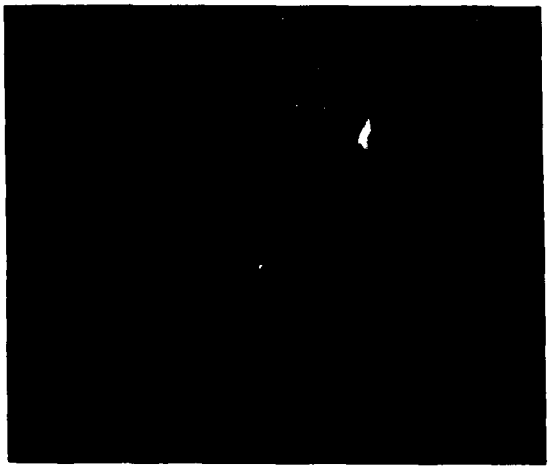

(c) CROSS-CORRELATION OUTPUT OF THE LETTER A AND THE BINARY HOLOGRAM (a)

Figure 9. Cross-Correlation of the Letter A and Binary Fourier Transform Hologram

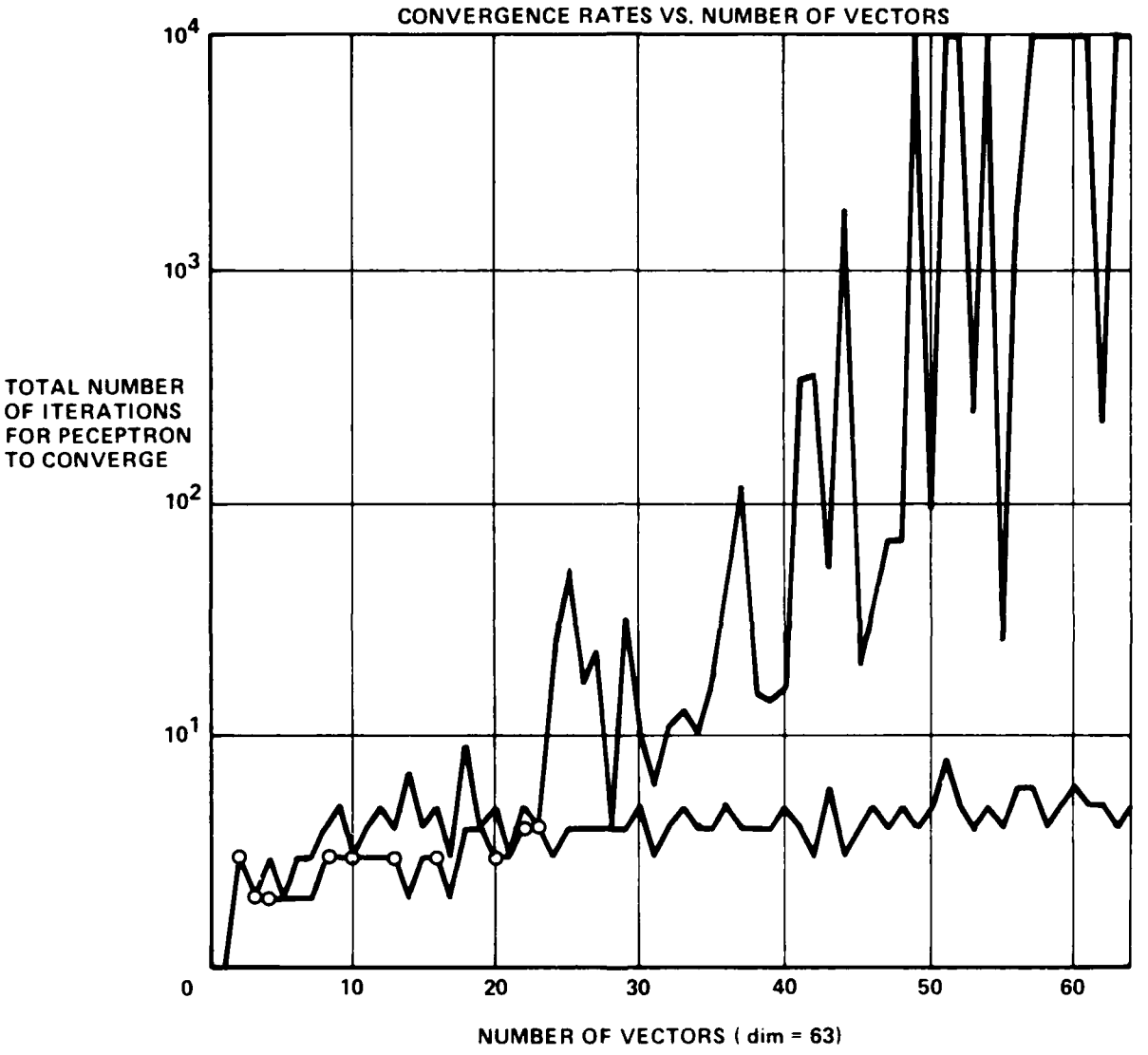

Figure 10. The Rate of Convergence of a Bipolar Perceptron (The Rate of Convergence of an Ordinary Perceptron of the Same Data Set is Also Plotted for Comparison. The Circles on the Plot are the Bipolar Vectors Generated by Taking the sgn [] of the Ordinary Perceptron that Dichotomize the Data Set Correctly)

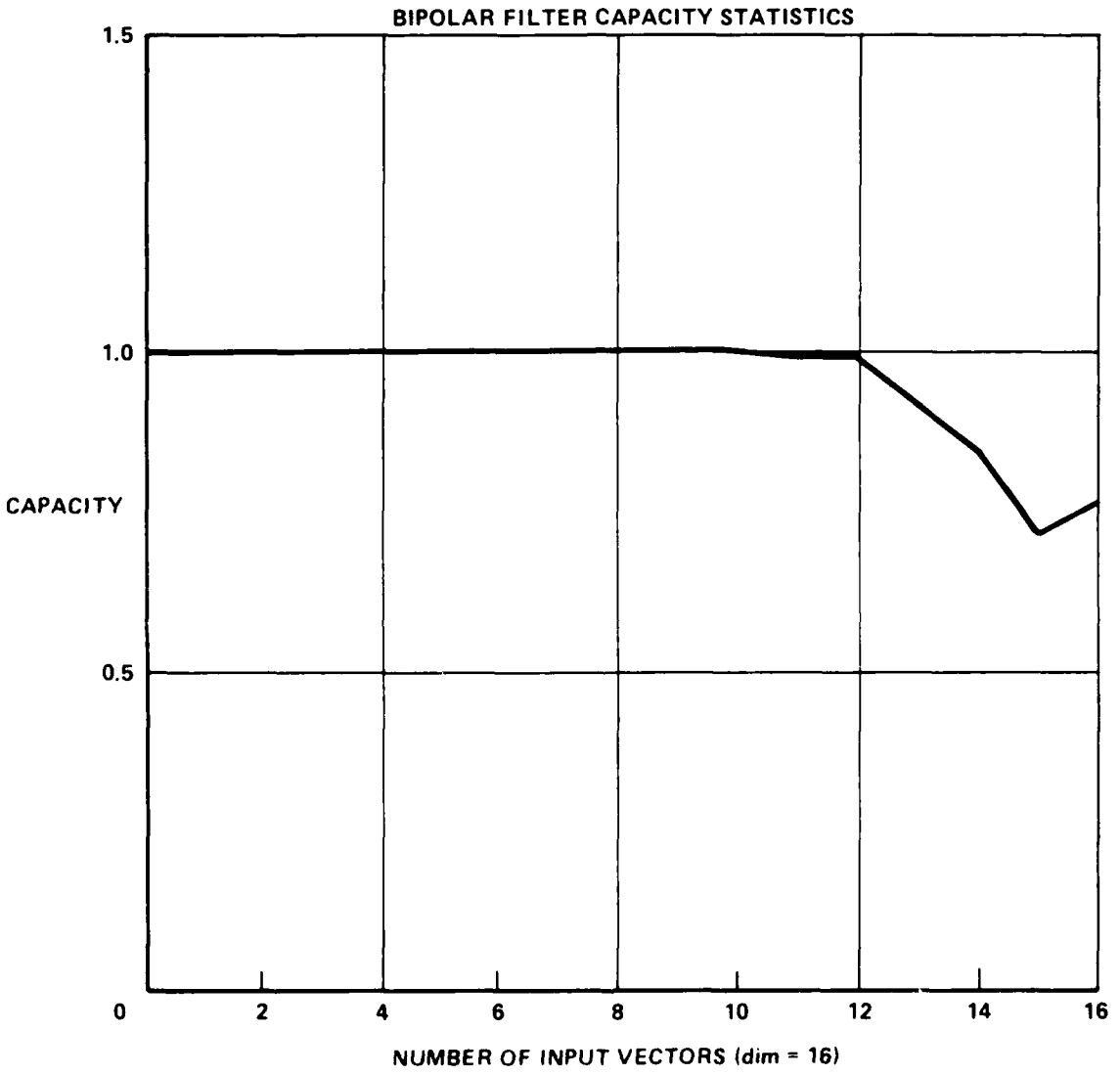

Figure 11. The Statistical Capacity of a Bipolar Filter With Non-Zero Threshold and Number of Weight Components Equal 16

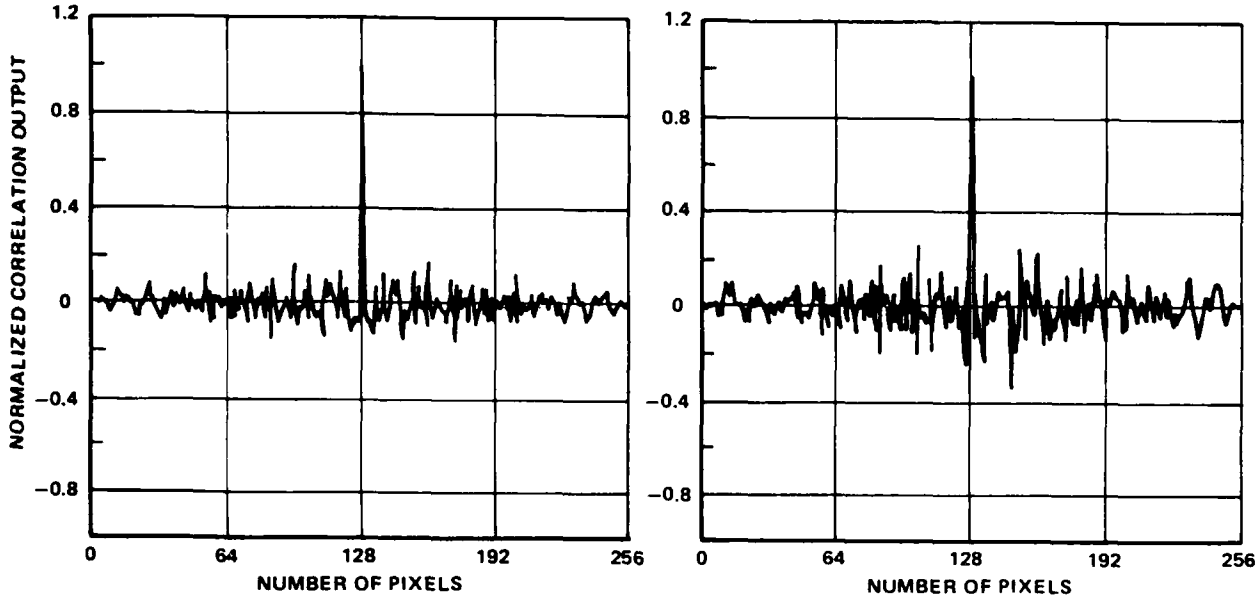

(a) CORRELATION OUTPUT (N = 128, M = 1)

(b) CORRELATION OUTPUT (N = 128, M = 2)

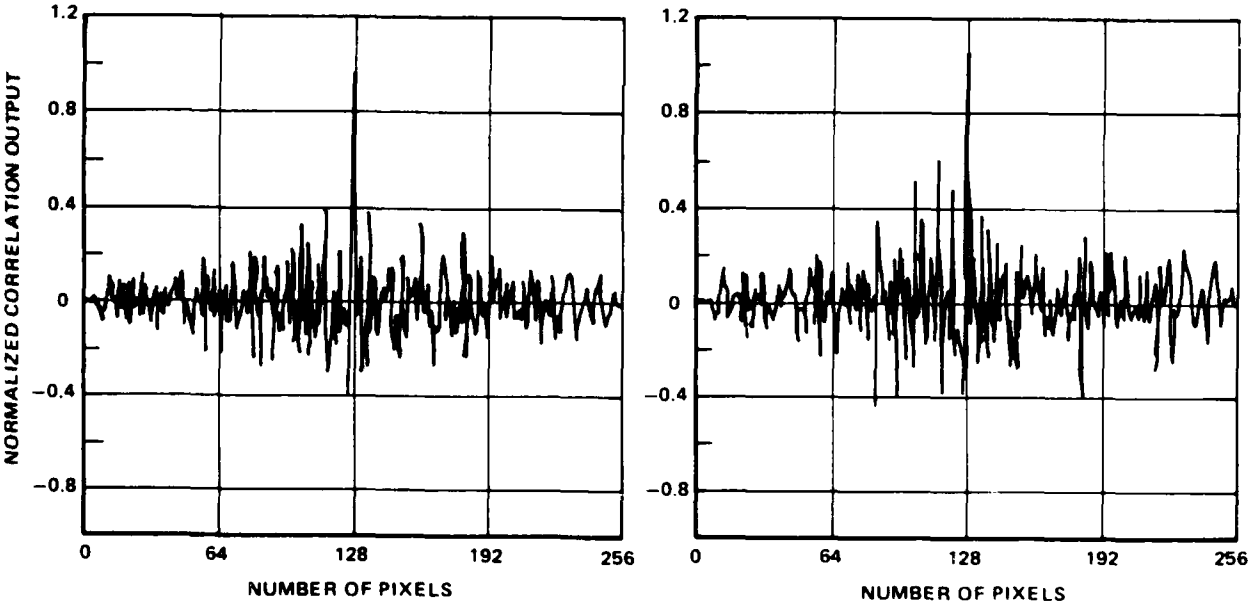

(c) CORRELATION OUTPUT (N = 128, M = 4)

(d) CORRELATION OUTPUT (N = 128, M = 6)

Figure 12. The Simulated Correlations of the Linear Weighted-Sum Filters of Different Number of Stored Vectors and Some of Their Stored Vectors (The Threshold Level for Recognition is One Half of the Energy of Each Vector)

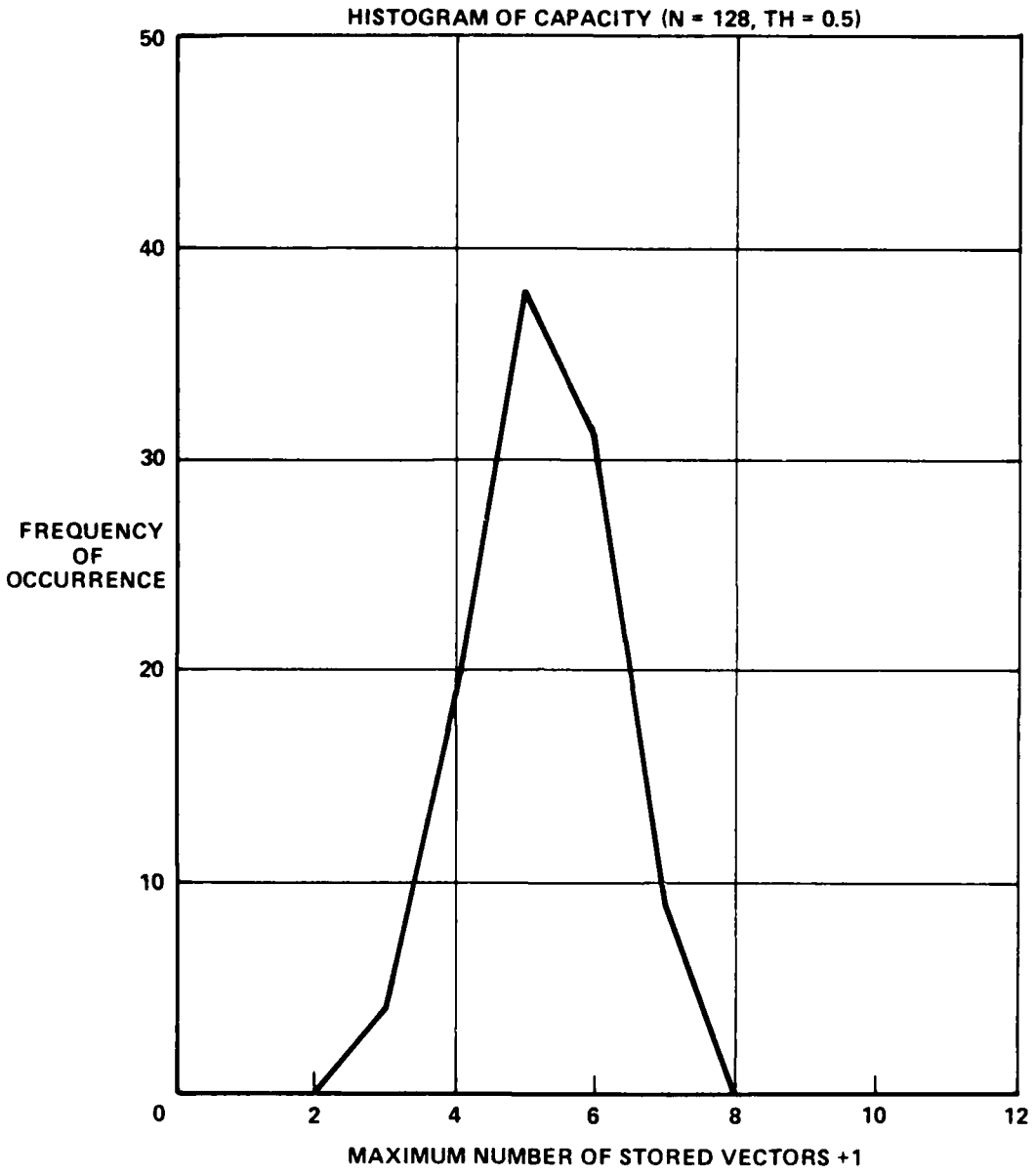

Figure 13. The Histogram of Storage Capacity Based on 100 Trials

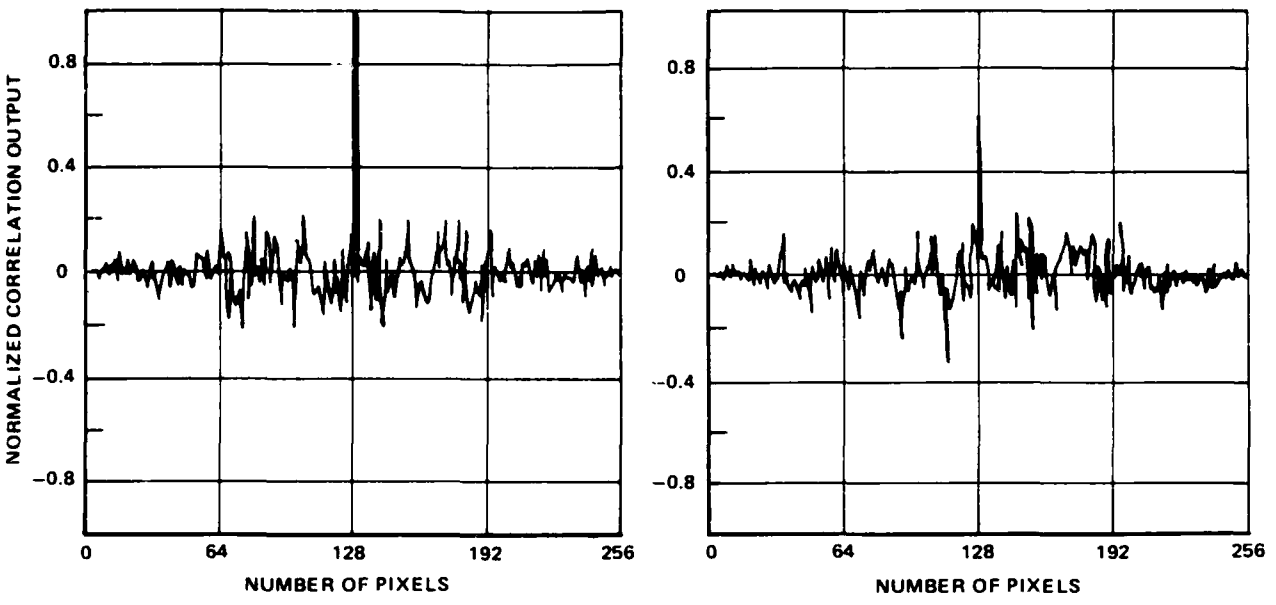

(a) CORRELATION WITH BIPOLAR FILTER (M = 1)

(b) CORRELATION WITH BIPOLAR FILTER (M = 2)

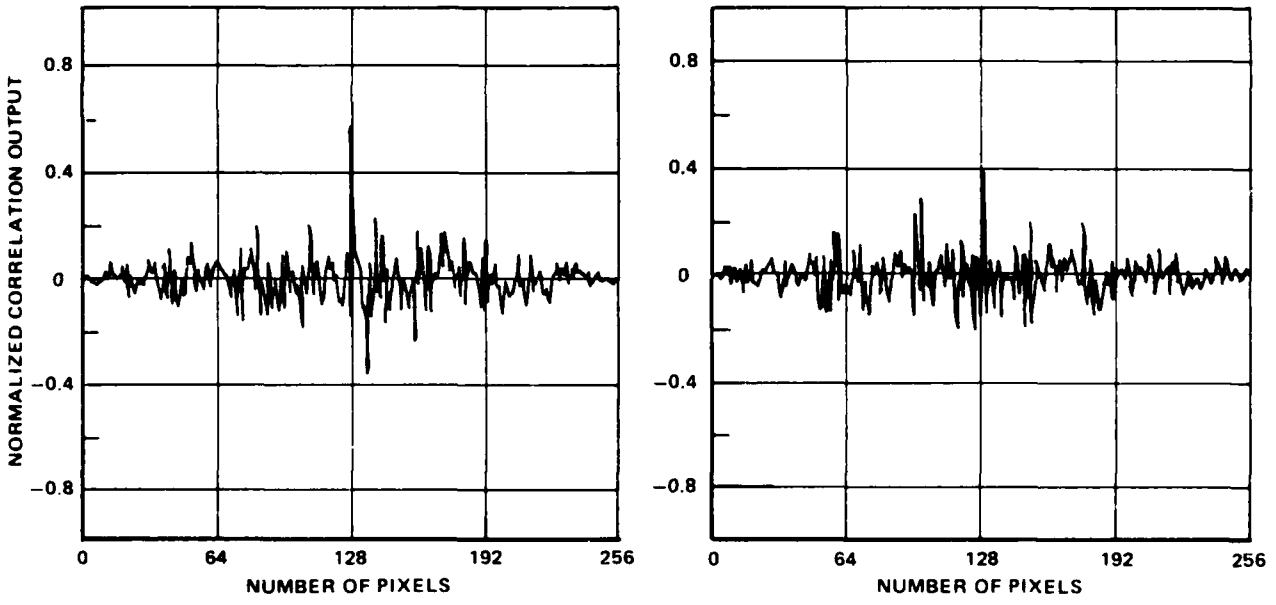

(c) CORRELATICN WITH BIPOLAR FILTER (M = 3)

(d) CORRELATION WITH BIPOLAR FILTER (M = 4)

Figure 14. Computer Simulated Correlations of Bipolar Weighted-Sum Filters of Different Number of Stored Vectors and Some of Their Stored Vectors (The Threshold Level for Recognition is One-Half of the Energy of Each Vector)

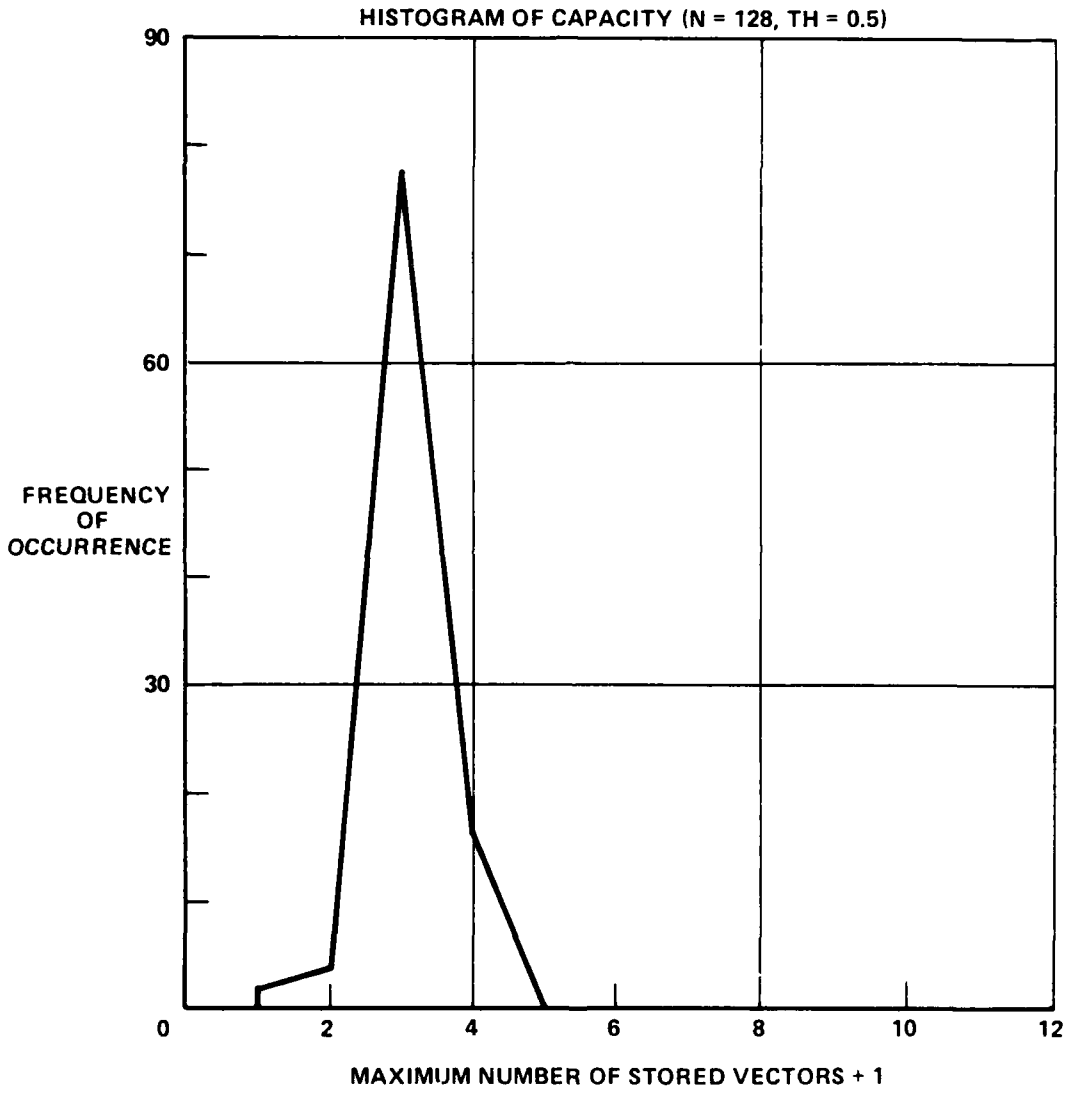

Figure 15. The Histogram of Storage Capacity of the Bipolar Weighted-Sum Filter Based on 100 Trials

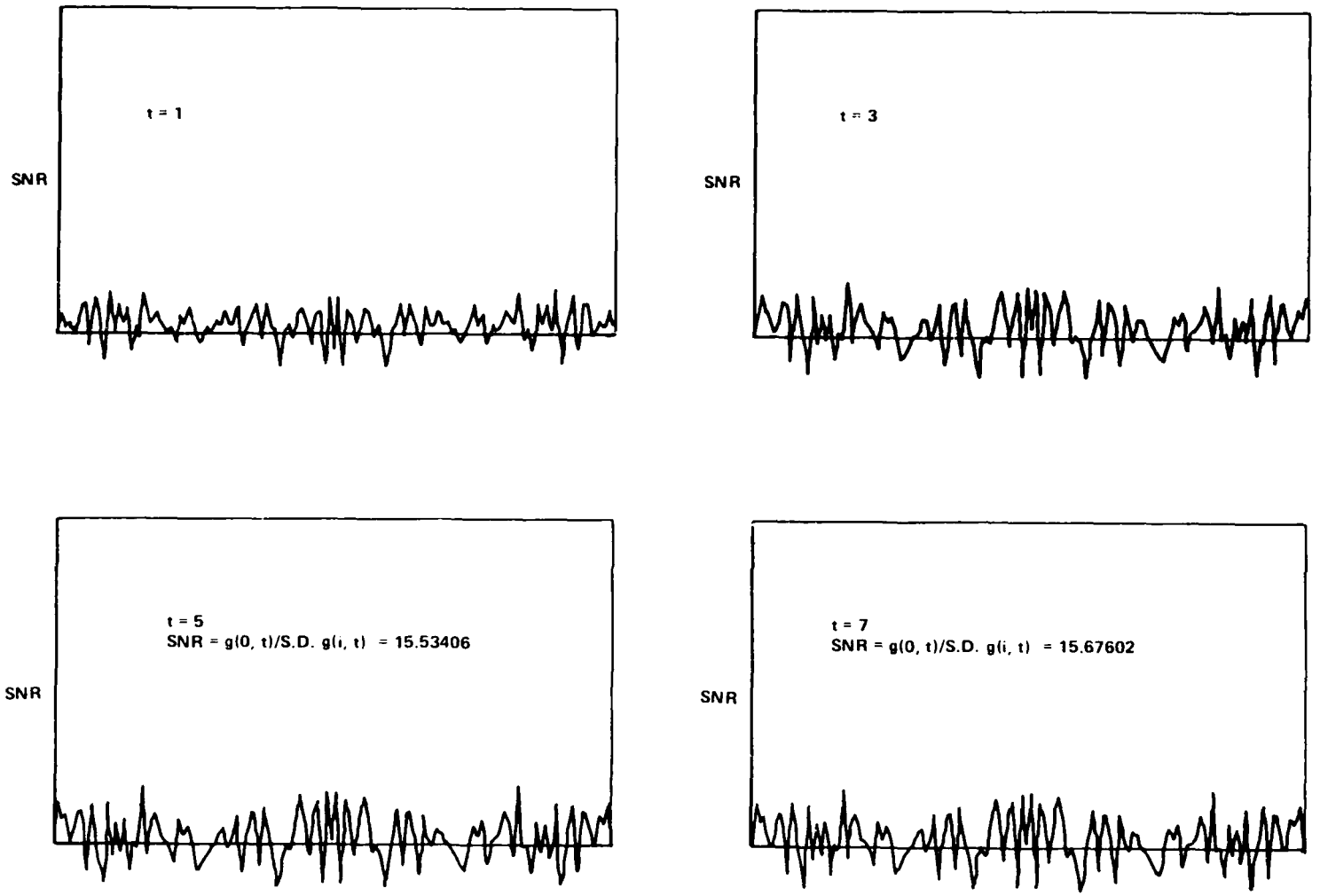

Figure 16. Numerical Evaluation of Bit-Slice Correlations at Different Time Integration Intervals

REFERENCES

1. A. Vander Lugt, Institute of Electrical and Electronic Engineers (IEEE) Transactions in Information Theory IT-10, 2 (1964).

2. D. Psaltis, E.G. Paek, and S.S. Vankatesh, Optical Engineering 23(6), 698 (1982).

3. Y.N. Hsu, H.H. Arsenault, and G. April, Applied Optics 21, 4012 (1982).

4. N.J. Nilson, Learning Machines: Foundations of Trainable Pattern-Classifying Systems, McGraw-Hill Book Company, New York, 1965.

END

DATE

FILMED

6-1988

DTIC